Isolated Gain Enhancement for Dual-Band C-Metaloop Antennas Using a Coplanar Compound Method

Hisamatsu Nakano, *Life Fellow, IEEE*, Tomoki Abe, *Member, IEEE*, Amit Mehta, *Senior Member*, *IEEE* and Junji Yamauchi, *Life Fellow, IEEE*

***Abstract*—When the circumference of a round metaloop antenna (RoMLA), made of C-type meta-atoms, is one guided wavelength ($1\lambda_g$) of the current on the loop, the RoMLA radiates a left-hand CP wave at frequency f_N and a right-hand CP wave at frequency f_H in the direction normal to the antenna plane. These CP waves have different maximum gains. This paper discusses enhancement in the small gain, not affecting the inherent large gain. Such uncorrelated enhancement in the gain, named the isolated gain enhancement (IsoGE), differs from conventional correlated gain enhancement (non-IsoGE). For IsoGE, a parasitic ring is inserted into the open space of the RoMLA, while maintaining the low-profile RoMLA structure on the order of $\lambda_0/100$ with λ_0 being the free-space operating wavelength. It is found that the ring finally transformed into a round patch is effective for the IsoGE, where the induced current on the patch contributes to increasing the small gain. The analysis, for the first time, shows that the axial ratio and VSWR are, respectively, less than 3 dB and 2 across the 3-dB gain bandwidths around f_N and f_H, as desired. Furthermore, the insertion of a square parasitic patch within the open space of a square metaloop antenna is also found to be effective for the IsoGE.**

***Index Terms*—circular polarization, dual-band metaloop antenna, meta-atom, uncorrelated gain enhancement**

I. Introduction

THE gain is one of the major characteristics for an antenna [1][2]. A loop antenna [3][4] located in free space radiates a bidirectional, circularly polarized (CP) beam with a small gain, when the loop circumference is one guided wavelength ($1\lambda_g$). This gain is increased by placing a conducting plate behind the loop antenna, as in a spiral antenna [5], where the distance between the plate and the loop is set to be $\lambda_0/4$ (λ_0 is the free-space wavelength at the design frequency). As the antenna height is reduced from $\lambda_0/4$ to realize a low-profile structure, the gain is decreased. However, recent study has revealed that this gain reduction can be mitigated if the conducting plate is replaced by an EBG reflector [6]-[10], where the antenna height is, for example, approximately $\lambda_0/10$.

Responding to the emergence of metamaterial [11]-[13], antennas are categorized into a natural antenna group and a metamaterial antenna (meta-antenna) group [14]. The propagation phase constant, β, for the current of the former has a positive value, and that of the latter has, at least, a negative value. Note that β for the current on the abovementioned loop antennas is positive, and hence these loop antennas (conventional loop antennas) belong to a natural antenna group. Also, note that a transmission line antenna that behaves like a β-negative (CL circuit, backward circuit) line in the low frequency band and a β-positive (LC circuit, forward circuit) line in the high frequency band [11] is categorized into a metamaterial-antenna group, based on the presence of the negative β current.

Recently, a flat square CP metamaterial loop (metaloop) antenna (SqMLA), which is made of C-type meta-atoms [15] and named C-SqMLA, has been created [16], where the antenna height is smaller than that for the EBG-backed loop antenna and is on the order of $\lambda_0/100$. It has been revealed that the SqMLA radiates a left-hand circularly polarized (LHCP) beam at a frequency (f_N) and a right-hand circularly polarized (RHCP) beam at a different frequency (f_H), i.e., the SqMLA acts as a dual-band anti-CP radiation element unlike conventional natural loop antennas. It has also been revealed that the gain for the SqMLA at f_N is smaller than that at f_H; however, it has been described that the smaller gain at f_N can be enhanced by adding a parasitic loop *above* the SqMLA [17]. Note that this antenna structure destroys the attained low-profile flat structure of the SqMLA, although the gain at f_N is increased.

As will be summarized in this paper, a round metaloop antenna (RoMLA), made of C-type meta-atoms and named a C-RoMLA, shown in Fig. 1, is known as a dual-band anti-CP antenna and suffers from a CP small gain at f_N. As done for the small gain of the SqMLA, the placement of a parasitic loop *above* the C-RoMLA is a technique of increasing the small gain at the cost of the attained low-profile flat antenna structure.

In contrast, increasing the small gain for the C-RoMLA at f_N in [18] is performed without using a parasitic element above the loop; this is done by increasing the antenna arm length.

Mannuscript received MM dd 2022, revised MM dd, 2022: Accepted MM dd, 2022. This work was supported in part by JSPS KAKENHI under Grant JP 21K04068. (*Corresponding author: Hisamatsu Nakano*).

H. Nakano (e-mail: hymat@hosei.ac.jp), T. Abe (e-mail: tomoki.abe.5r@stu.hosei.ac.jp), and J. Yamauchi (e-mail: j.yma@hosei.ac.jp) are with the Department of Science and Engineering, Hosei University, Koganei, Tokyo, Japan 184-8584.

A. Mehta is with the College of Engineering, Swansea University, Swansea SA1 8EN, U.K. (e-mail: a.mehta@seansea.ac.uk).

Digital Object Identifier 10.1109/TAP.xxxxxx

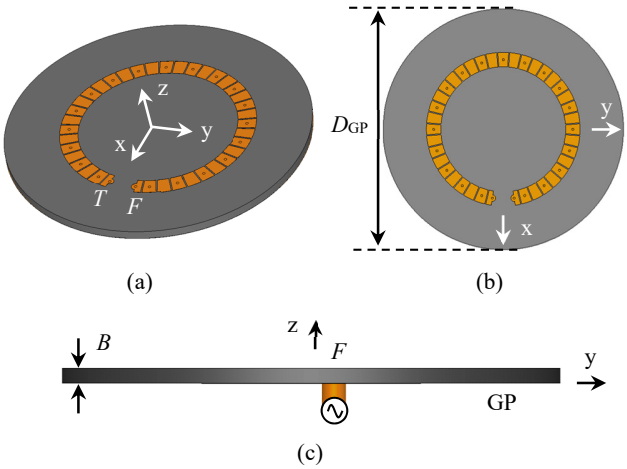

Fig. 1. Round metaloop antenna made of C-type metaatoms, C-RoMLA, where D_{GP} = 110 mm. (a) Perspective view. (b) Top view. (c) Side view.

However, the increase in the arm length causes complex antenna design and high fabrication cost; in addition, another gain at f_H changes with additional arm length. Such enhancement is called the *non-isolated gain enhancement* (non-IsoGE) because it is against the definition of the *isolated gain enhancement* (IsoGE) where one of the two gains for a dual band anti-CP antenna is enhanced, not affecting the other gain. Note that IsoGE provides more freedom than the non-IsoGE in the design of CP communication systems.

Table I summarizes the gain enhancement (relative to the initial gain) of the prior CP metamaterial antennas [16], [18], [19], [20], [21], where G_{LH} and G_{RH} denote the LHCP and RHCP gains, respectively. The antenna structure using C-type meta-atoms [16], [18], [19], [21] acts as a dual-band antenna, and the antenna structure using quasi-N-type meta-atoms [20] also acts as a dual-band antenna. On the other hand, the antenna structure using N-type meta-atoms [19] acts as a single-band antenna. For comparison, the characteristics of the antenna realized in this paper is also presented in advance. Table I points out that the small gain of the conventional dual-band metamaterial antennas is increased, while decreasing undesirably the inherent/initial large gain. The prior work has not succeeded in an uncorrelated gain enhancement, i.e., IsoGE. Note that the G_{LH} in the initial stage of the antenna in [20] using quasi-N-type meta-atoms is decreased in the final stage, while G_{RH} is increased. It follows that all prior antennas in Table I, except for the present work, do not realize IsoGE.

In this context, this paper investigates the IsoGE for a dual-band anti-CP metaloop antenna to obtain more freedom in the gain control. For this, a parasitic ring and its extremity (patch) are placed within the open space of the loop, having the same antenna height as the loop (coplanar compound method). The present paper clarifies the radiation characteristics of the metaloop antenna with the patch, including the VSWR, axial ratio, gain, and radiation pattern, for the first time.

The paper is composed of six sections. Section II revisits the C-RoMLA and briefly summarizes the basic radiation characteristics, which are obtained using an EM simulation tool [22]. The simulation clarifies an issue of gains G_{LH} and G_{RH}. Section III proposes placement of a conducting ring within the open space of the loop; we name this compound the RoMLA-RING and investigate the gain behavior at f_N and f_H, changing inner radius r_{ring} of the ring that has outer radius r_{RING}, i.e., changing ring width w_{RING} (= r_{RING} − r_{ring}). The investigation reveals that the ring transformed into a patch (at the extremity of the ring width: r_{ring} = 0, or w_{RING} = r_{RING}) is effective for the IsoGE. The RoMLA with the patch is named the RoMLA-PATCH. Section IV confirms the validity of the analyzed antenna characteristics obtained in section III by measuring fabricated RoMLA-PATCHs. For further information, section V realizes the IsoGE for an SqMLA using the co-planar compound method, where a square parasitic patch is placed within the open space of the loop. Finally, section VI summarizes the obtained results in this paper.

Important comments C-1, C-2, and C-3 are made here to further clarify the novelty and effectiveness of the presented RoMLA-RING and RoMLA-PATCH, in addition to the difference in the patches used in [19] and those in the presented paper. C-1: Table II summarizes representative examples of the gain enhancement of conventional natural CP antennas [23], [24], [25], [26], [27]. Each operates across only a single band (N_{BND} = 1) with single polarization (N_{POLAR} = 1), where the number of parasitic elements is equal to one or more than four ($N_{paras} \geq 4$). In contrast, the present antenna (whose details are

Table I. Examples of gain enhancement of CP metamaterial antennas. Arrows show the increased, decreased, and unchanged gains relative to the initial gains.

	Antenna shape	Meta-atom	Number of operation bands	Initial gain (G_{LH0}/G_{RH0})	Increased gain (G_{LH}/G_{RH})	IsoGE	Parasitic elements to increase the gain
[16]	Square	C-type	Dual	−1.5 dBi/3.0 dBi	NA	NA	Absent
[18]	Round	C-type	Dual	≈5.5 dBi/≈8.5 dBi	↑ ≈7.0 dBi/≈7.0 dBi ↓	No	Absent
[19]	Round Round	N-type C-type	Single Dual	NA/NA NA/NA	11.7 dBi/NA 9.0 dBi/NA	NA NA	Absent Absent
[20]	Round	Quasi-N-type	Dual	≈7.0 dBi/≈3.0 dBi	↓ ≈6.0 dBi/≈6.0 dBi ↑	No	Absent
[21]	Curl	C-type	Dual	≈5.5 dBi/≈8.5 dBi	↑ ≈7.0 dBi/≈7.0 dBi ↓	No	Absent
This work	Round Square	C-type C-type	Dual Dual	5.0 dBi/9.0 dBi 3.5 dBi/9.2 dBi	↑ 8.4 dBi/≈9.0 dBi → ↑ 7.8 dBi/9.2 dBi →	Yes Yes	Round patch Square patch

Table II. Examples of gain enhancement of natural CP antennas.

	Number of operation bands	Antenna area	Height	Gain	Fed antenna	Shape of parasitic patches	Number of parasitic patches	Coplanar compound
[23]	Single	$2.10\lambda_0^2$	$0.028\lambda_0$	12.5 dBi	Loop	Rectangular	8	Yes
[24]	Single	$0.85\lambda_0^2$	$0.028\lambda_0$	9.8 dBi	Loop	Square	8	Yes
[25]	Single	$1.27\lambda_0^2$	$0.116\lambda_0$	≈8 dBi	Patch	Rectangular	4	Yes
[26]	Single	$0.64\lambda_0^2$	$0.30\lambda_0$	8.6 dBi	L-shaped line	Square	1	No
[27]	Single	$2.98\lambda_0^2$	$0.618\lambda_0$	14.6 dBi	Patch	Square	25	No

described later) is characterized by $N_{BND} = 2$, $N_{POLAR} = 2$, and $N_{paras} = 1$. This means that the present antenna extends capability of CP communication systems, having a simple structure. Note that antennas in [26], [27] lose a low-profile structure. Also, note that the natural antennas in Table II are unrelated to IsoGE because of $N_{BND} = 1$; in addition, to the best of authors' knowledge, there has not been work on the IsoGE for natural and metamaterial CP antennas using a parasitic coplanar ring or its extremity (patch). Hence, it is worth investigating the combination of a metamaterial dual-band antenna and a natural parasitic ring from a viewpoint of the IsoGE.

C-2: The research purpose in [19] is to investigate the influence on the radiation characteristics of additional device that is inserted into the open space of an N-RoMLA, made of N-type meta-atoms [15]. The loop circumference is unusually large (compared with $1.7\lambda_0$ of the work in this paper): $3\lambda_0$, $4\lambda_0$, and $5\lambda_0$ with λ_0 being the free-space wavelength at a design low frequency. The additional device is generalized/substituted by a patch, which is not aimed to increase the gain. It follows that the research purpose, process, and findings for the large N-RoMLA with a patch in [19] obviously differ from those for the C-RoMLA to be discussed in this paper. The contents of paper [19] have nothing to do with IsoGE, although it shows that the gain for the N-RoMLA and C-RoMLA without a parasitic patch is increased as the loop circumference is increased.

C-3: The C-RoMLA in this paper exceeds the N-RoMLA [19] in the antenna performance; the former can operate as a dual-band anti-CP antenna: $N_{BND} = 2$ and $N_{POLAR} = 2$, while the latter only operates across a single band with single polarization: $N_{BND} = 1$ and $N_{POLAR} = 1$. Hence, this paper focuses on the C-RoMLA based on this advantage. From now on, "RoMLA" and "SqMLA" mean "C-RoMLA" and "C-SqMLA," respectively, unless otherwise noted, i.e., both are made of C-type meta-atoms [15], which are realization of the cells for a CRLH transmission line [11].

II. Brief Summary and Clarification of Gain Issue for an RoMLA

The fundamental information on RoMLA is available from [18], [20]. Therefore, this section presents the minimum information required for understanding this paper.

The dispersion diagram for the C-type meta-atom [15], used as a radiation element for the RoMLA in Fig. 1, is shown in Fig. 2. Note that the configuration and parameters of the C-type meta-atom are, respectively, summarized in Appendix-Fig. A and Appendix-Table.

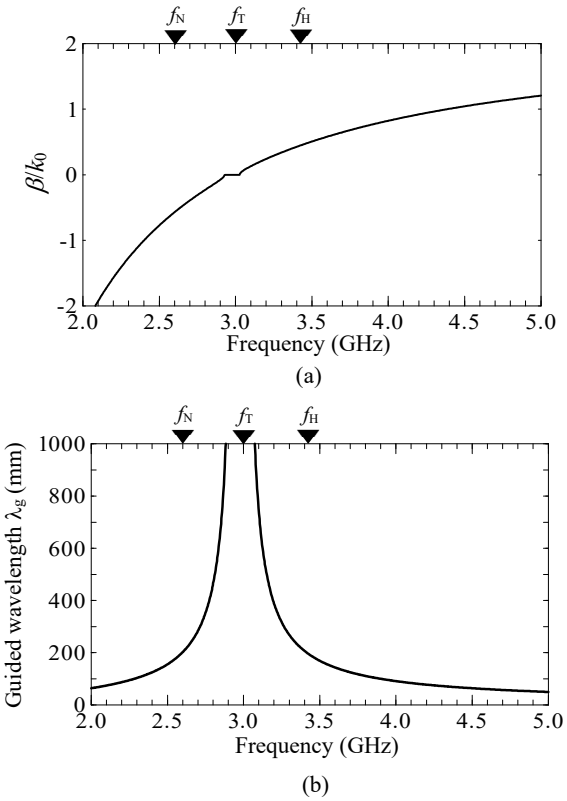

Fig. 2. C-type meta-atom. (a) Dispersion of β/k_0, where k_0 is the phase constant in the free space, and β is the phase constant of current on the meta-atom. (b) Guided wavelength λ_g of the current on the meta-atom.

The center line of the loop has radius R_{MLA}, and both the ground plane and the dielectric substrate have the same radius of $R_{GP} = D_{GP}/2$ (= 55 mm). The RoMLA is excited at point F, to which the inner conductor of a coaxial line is connected. The end of the loop, T, is connected by a vertical conducting pin (diameter of $2r_{VIA}$ = 1.0 mm) to the ground plane through resistive load R_B (= 60 ohms). If the resistive load R_B is not inserted, the current at point T on the loop does not completely die out and travels back to the feed point F. By absorption of the remaining current at point T using R_B, the RoMLA becomes a traveling wave antenna (a leaky wave antenna) of a one-way current from point F. Note that the radiation efficiency and the axial ratio under the conditions of matched load R_B and fixed

loop circumference are affected by the propagation attenuation constant of the current (which is frequency-dependent) related to the arm width and thickness of dielectric substrate relative to the operating wavelength.

The circumference of the loop, $2\pi R_{MLA} \equiv C_{MLA}$, as a function of frequency f is shown in Fig. 3, where C_{MLA} is normalized to the guided wavelength λ_g shown in Fig. 2(b). Note that a circularly polarized (CP) broadside beam appears at the frequency where the loop circumference is one guided wavelength ($C_{MLA} = 1\lambda_g$) and close to one guided wavelength ($C_{MLA} \approx 1\lambda_g$).

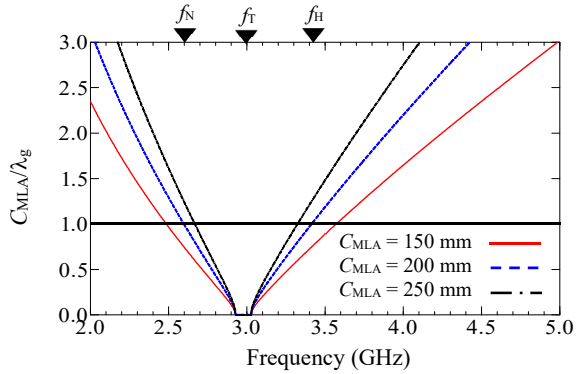

Fig. 3. Relative loop circumference C_{MLA}/λ_g as a function of frequency with loop circumference C_{MLA} as a parameter.

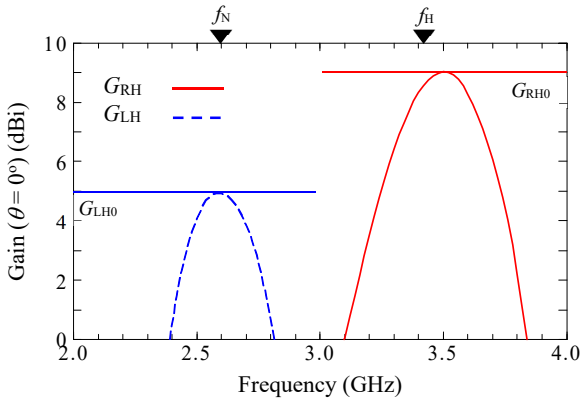

Fig. 4. Frequency response for the gain of RoMLA.

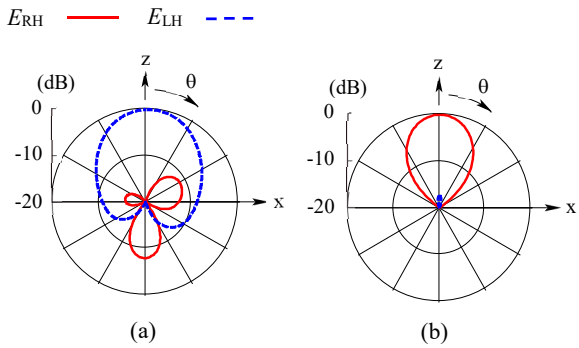

Fig. 5. Radiation pattern for RoMLA when the gain is the maximum. (a) 2.6 GHz. (b) 3.5 GHz.

There are two frequencies, called nion frequency f_N and hion frequency f_H, where the loop circumference equals $1\lambda_g$ and meets the requirement of CP broadside/axial radiation. For example, when a value of C_{MLA} = 200 mm is chosen, nion frequency f_N is 2.60 GHz and hion frequency f_H is 3.42 GHz. The following discussion is performed using C_{MLA} = 200 mm as a representative example. This circumference is approximately $1.7\lambda_0$ at f_N, which allows a parasitic element to exist within the open space of the loop and increase the antenna gain, as will be discussed in Section III.

Fig. 4 shows the simulation results of the frequency response of the gain for the RoMLA in the z-direction. The maximum gain for an LHCP wave, G_{LH}, appears at 2.6 GHz (= f_N), while the maximum gain for an RHCP wave, G_{RH}, appears at 3.5 GHz ($\approx f_H$), as expected. The values of these gains are not the same. The reason for this unbalance is attributed to the difference in the *electrical* antenna size with respect to the free-space wavelength; C_{MLA}/λ_0 at 2.6 GHz is smaller than that at 3.5 GHz. This brings a difference in the radiation patterns at the two frequencies of f_N and f_H, resulting in the different gains.

For reference, Fig. 5 shows the simulated radiation patterns when the maximum gains of G_{LH} and G_{RH} (denoted as initial gains G_{LH0} and G_{RH0}, respectively) appear; these radiation patterns are normalized to the respective maximum intensities in the z-direction, and E_{LH} and E_{RH} denote the LHCP and RHCP radiation field components, respectively. The current on the loop at 2.6 GHz has a negative propagation phase constant ($\beta < 0$, leading to a progressive phase progression) and behaves as if it flows clockwise, resulting in E_{LH} being a principal field component. In contrast, the principal field component at 3.5 GHz near f_H is E_{RH}, resulting from the current of a positive propagation phase constant ($\beta > 0$, leading to a regressive phase progression and a counterclockwise current flow).

III. IsoGE for The RoMLA Using a Coplanar Compound Method

A. Gain

As summarized in Section II, the representative RoMLA radiates a CP unidirectional beam in the z-direction and has two different maximal gains of G_{LH0} and G_{RH0}, where $G_{LH0} < G_{RH0}$. The challenging work in this paper is to realize the IsoGE for the RoMLA, i.e., to increase the small gain G_{LH0} appearing at/near f_N, not affecting the inherent/initial large gain G_{RH0} appearing at/near f_H. Note that, as described in Introduction, the N-RoMLA in [19] is a single band antenna and hence it does not need to discuss IsoGE; remember that IsoGE applies to only a dual-band CP antenna.

To enhance the gain G_{LH0} (initial gain), a conducting parasitic ring is printed within the RoMLA, as shown in Fig. 6(a). This compound is denoted as RoMLA-RING. The height of the ring is the same as that of the loop (coplanar compound method). The ring is specified by outer ring radius r_{RING}, inner ring radius r_{ring}, and ring width $w_{RING} = r_{RING} - r_{ring}$. Fig. 6(b) shows the gain behavior observed at 2.6 GHz = f_N and 3.5 GHz ≈ f_H as a function of w_{RING}, where r_{RING} is chosen to be 19.0 mm and fixed: r_{RING} = 19.0 mm. Note that this ring radius r_{RING} is close

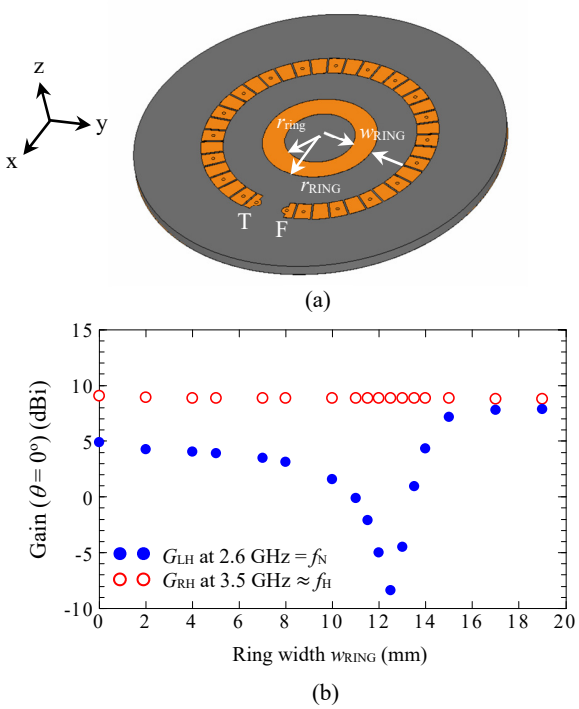

Fig. 6. RoMLA-RING. (a) Configuration, where the circumference of RoMLA is C_{MLA} = 200 mm and the outer radius of a ring is r_{RING} = 19.0 mm. (b) Gains observed at 2.6 GHz = f_N and 3.5 GHz ≈ f_H with ring width w_{RING} as a parameter.

to the radius r_{exp} (= 19.5 mm) in the following Eq. (1) for a round patch antenna working in TM^z_{110} mode at $f = f_N$ = 2.6 GHz [28], where r_{exp} is obtained by solving Eq. (1) after substituting Eq. (2) into Eq. (1).

$$r_{exp} = \frac{r_{eff}}{\sqrt{1+\frac{2B}{\pi\epsilon_r r_{exp}}\left(\ln\frac{\pi r_{exp}}{2B}+1.7726\right)}} \quad (1)$$

where

$$r_{eff} = \frac{1.8412}{2\pi C_0 f\sqrt{\varepsilon_r}} \quad (2)$$

with C_0 being the velocity of light.

The situation where width w_{RING} is zero means that the ring does not exist, and the situation where w_{RING} equals the outer ring radius r_{RING} (hence, inner ring radius r_{ring} = 0) means that the ring is transformed into a round patch. Fig. 6(b) points out that, with increase in w_{RING}, the gain G_{LH} at f_N decreases from the initial gain G_{LH0} to a minimum value; after passing it, the gain G_{LH} increases and reaches a maximum value, which is larger than G_{LH0}. During the change in w_{RING}, the large gain near f_H remains unchanged. Thus, the IsoGE is realized when w_{RING} = r_{RING} (patch structure) and w_{RING} ≈ r_{RING}.

Based on the usefulness of the patch structure for the IsoGE, the frequency response of gain is investigated with patch radius r_{PATCH} as a parameter. Fig. 7 depicts the simulation results of the gain. It is found that all maximum gains of G_{LH} for the RoMLA-PATCH is larger than the initial G_{LH0}, while the maximum gain of G_{RH} remains unchanged. The increase in G_{LH} is more than 3 dB, depending on r_{PATCH}. This is due to the strong

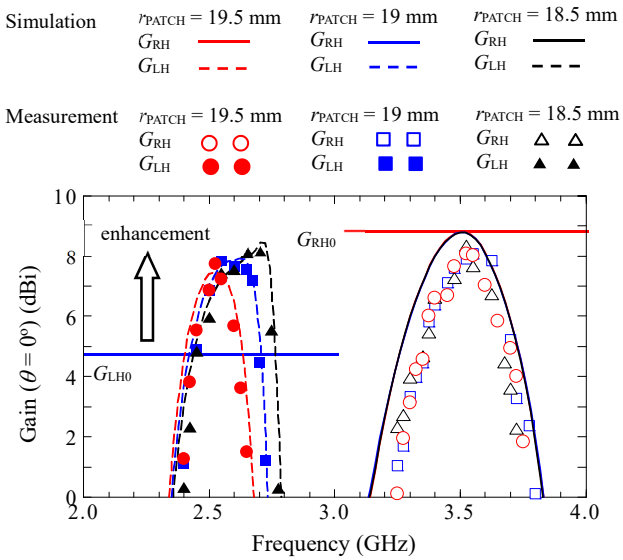

Fig. 7. Gain of RoMLA-PATCH as a function of frequency with patch radius r_{PATCH} as a parameter, where C_{MLA} = 200 mm. Note that the simulated RHCP gains (G_{RH}) for three r_{PATCH} cases are superimposed.

Table III. Comparison between r_{PATCH} and r_{exp}.

f	r_{exp}	r_{PATCH}	$\frac{r_{exp}-r_{PATCH}}{r_{PATCH}}$
2.50 GHz	20.3 mm	19.5 mm	4.1%
2.60 GHz	19.5 mm	19.0 mm	2.6%
2.70 GHz	18.7 mm	18.5 mm	1.1%

coupling of the parasitic patch to the RoMLA, in other words, the generation of the currents on the patch.

Table III summarizes the difference between patch radius r_{PATCH} where gain G_{LH} is maximal at frequency f (found in Fig. 7) and r_{exp} given by Eq. (1) at the same frequency f. As seen from the Table, Eq. (1) is useful to infer the patch radius r_{PATCH} for strong coupling.

To provide deep insight on the coupling state, Figs. 8(a) and (b) show the frequency-domain electric field distributions (FreqD E-distributions) for the RoMLA itself (without a patch) and RoMLA-PATCH, respectively. Both are observed at 2.7 GHz. It is clear that the electric field spreads out within the open space of the RoMLA due to coupling of the patch to the RoMLA. For supplementary information, Fig. 8(c) shows the FreqD E-distribution when the patch is short-circuited by a single conducting pin extending from the center point of the patch to the ground plane. The behavior in Fig. 8(c) is found to be almost the same as that in Fig. 8(b), because the electric field intensity around the z-axis in Fig. 8(b) is extemely weak and hence the coupling is not affected by the presence of the conducting pin. However, when the outer edge of the patch is short-circuited by numerous pins, the resonance disappears, as shown in Fig. 8(d), where 32 pins are used. Note that the FreqD E-distribution at 2.7 GHz, Fig. 8(b), is changed into that shown

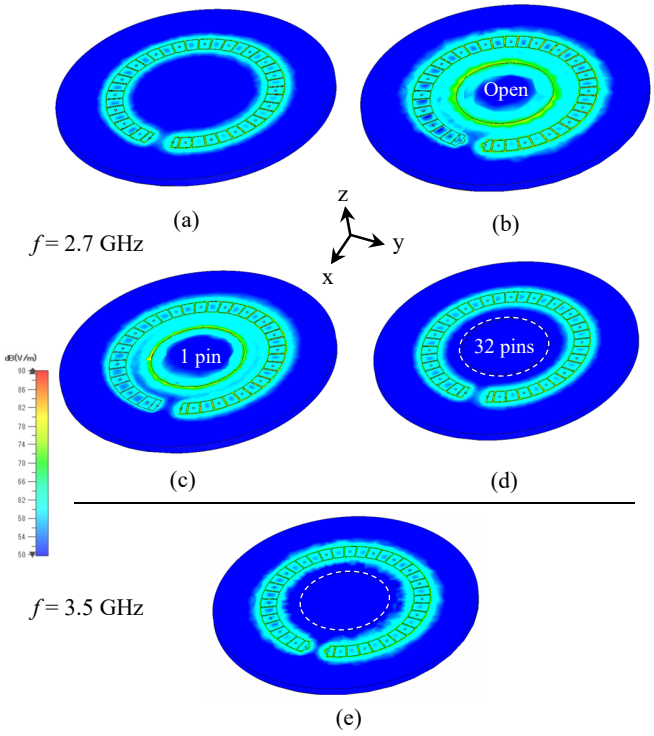

Fig. 8. Frequency-domain electric field distribution (FreqD E-distribution) at 2.7 GHz and 3.5 GHz. The patch has a radius of r_{PATCH} = 18.5 mm. The observation frequency in Fig. (a) to (d) is 2.7 GHz, and that in Fig. (e) is 3.5 GHz. (a) RoMLA in the absence of the patch. (b) RoMLA-PATCH, where the patch is open-circuited. (c) RoMLA-PATCH, where the patch is short-circuited by a single center conducting pin. (d) RoMLA-PATCH, where the edge of the patch is short-circuited by 32 conducting pins. (e) RoMLA-PATCH, where the patch is open-circuited at 3.5 GHz.

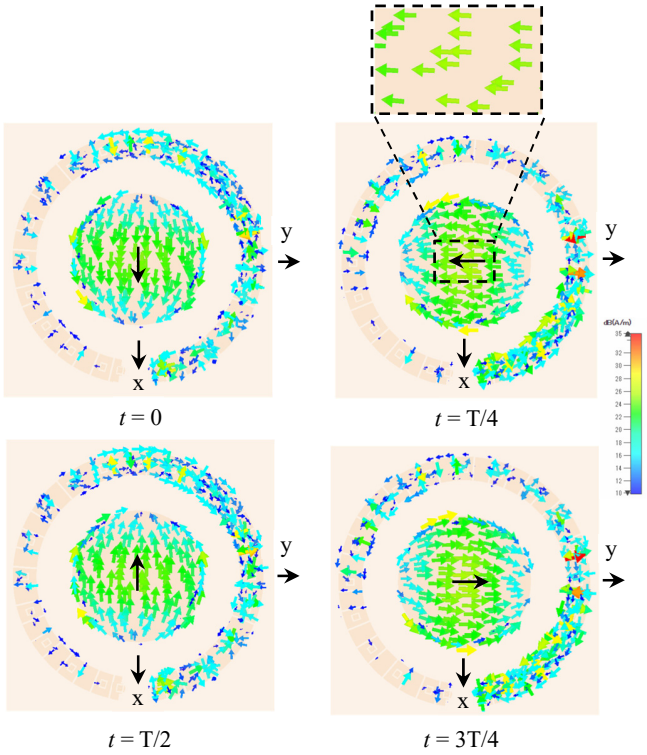

Fig. 9. Time-domain current distribution for the RoMLA-PATCH, where the patch radius is r_{PATCH} = 18.5 mm. T is one time-periodicity. At 2.7 GHz, where $\beta < 0$.

in Fig. 8(e) when frequency is changed to 3.5 GHz. It is confirmed that the patch has no coupling of the RoMLA, resulting in maintening the initial large gain G_{RH0}.

We focus on the time-domain current distribution (TimeD J-distribution) for the RoMLA-PATCH in the coupling state at 2.7 GHz, because of no effect of the patch on the large gain G_{RH0} at 3.5 GHz. Fig. 9 shows the TimeD J-distribution at 2.7 GHz. It is found that the currents on the parasitic patch, generated by coupling to the loop, are in the same direction. These rotate *clockwise,* as the current on the loop. As a result, the enhancement of the LHCP gain G_{LH} is realized.

B. Radiation pattern and input characteristic

In addition to the gain, other characteristics for the RoMLA-PATCH are investigated in this subsection, where the parasitic patch radius is set to be r_{PATCH} = 18.5 mm as a representative example.

Fig. 10 shows the radiation pattern when the gains G_{LH} and G_{RH} for the RoMLA-PATCH reach respective maximum values. The radiation pattern at 2.7 GHz has an E_L-half-power beam width (HPBW) of 63°, which is narrower than that of 70° in Fig. 5(a). This is consistent with antenna theory that a narrower HPBW leads to a higher directivity (gain). Note that the E_R-HPBW in Fig. 10(b) and that in Fig. 5(b) are almost the same (45°), resulting in no remarkable change in the gain G_{RH}, as shown in Fig. 7, where G_{RH}'s for three r_{PATCH} cases are superimposed.

Fig. 11 shows the frequency response of the axial ratio (AR) for the RoMLA-PATCH. The shaded area denotes the frequency region for 3-dB gain bandwidth, GBW. It is found that the AR across the LHCP GBW is stable with a value of less than 3 dB. This holds for the AR across the RHCP GBW. As additional information, the simulation results in the absence of the patch (i.e., RoMLA itself) is also shown in Fig. 11. A comparison of the axial ratios for the RoMLA-PATCH and the

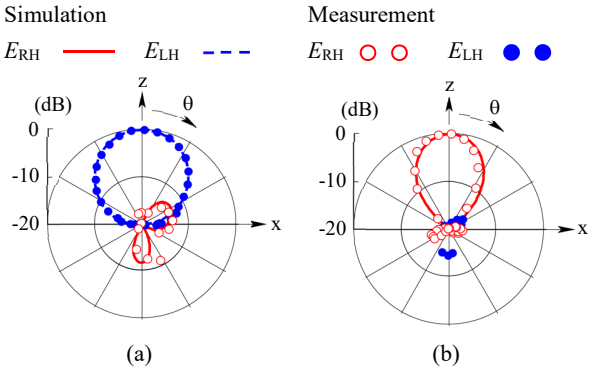

Fig. 10. Radiation pattern for the RoMLA-PATCH when the gains G_{LH} and G_{RH} reach respective maximum values, where the patch radius is r_{PATCH} = 18.5 mm as a representative example. (a) At 2.7 GHz. (b) At 3.5 GHz.

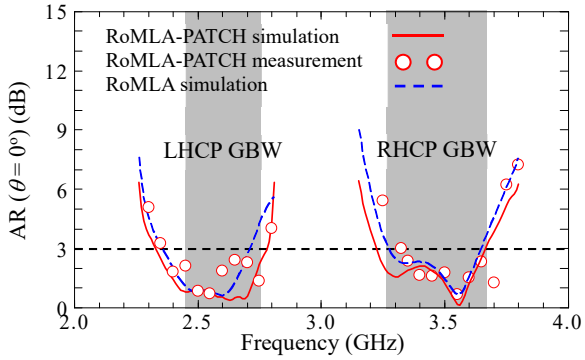

Fig. 11. AR for the RoMLA-PATCH, where the patch radius is r_{PATCH} = 18.5 mm. The AR for the RoMLA is also illustrated as additional information.

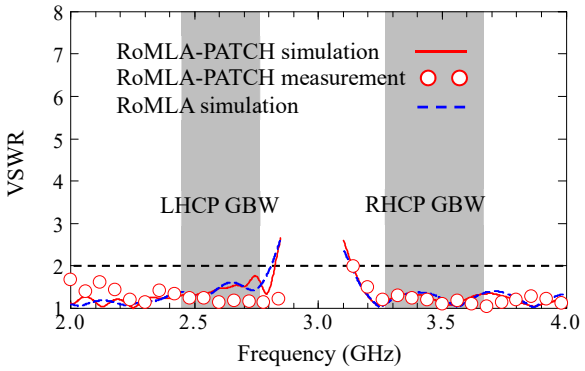

Fig. 12. VSWR for the RoMLA-PATCH, where the patch radius is r_{PATCH} = 18.5 mm. The VSWR for the RoMLA in the absence of the patch is also illustrated as additional information.

RoMLA reveals that the inserted patch does not remarkably affect the axial ratio for the RoMLA.

The frequency response of the input characteristic in terms of the VSWR for the RoMLA-PATCH is shown in Fig. 12. For comparison, the VSWR for the RoMLA in the absence of the patch (i.e., RoMLA itself) is also shown in this figure. It is found that the presence of the patch does not deteriorate the VSWR, as in the case of the axial ratio. The VSWR across the 3-dB gain bandwidth is found to be desirable with a value of less than 2.

As mentioned in section II, the arm end of the loop is terminated by resistive load R_B, which absorbs non-radiated power remaining at point T. The ratio of the radiated power to the input power is called the radiation efficiency, η_{RAD}. Fig. 13 shows the simulation results of the radiation efficiency for the RoMLA-PATCH. For comparison, the radiation efficiency of the RoMLA in the absence of the patch (i.e., RoMLA itself) is also presented. It is found that the insertion of the patch into the RoMLA increases η_{RAD} around nion frequency f_N, while almost maintaining η_{RAD} around hion frequency f_H. These results, obtained using the EM simulation tool [22], are in good agreement with those obtained using an estimation equation specified by S parameters.

$$\eta_{RAD} \approx 1 - |S11|^2 - |S21|^2 \quad (3)$$

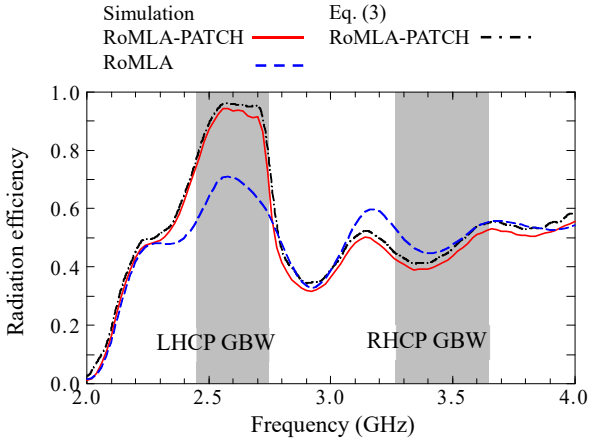

Fig. 13. Radiation efficiency for the RoMLA-PATCH, where the patch radius is r_{PATCH} = 18.5 mm. The radiation efficiency for the RoMLA in the absence of the patch is also illustrated as additional information.

where the dielectric loss and conducting loss along the loop are assumed to be negligibly small. Simulation for S21 by [22] is performed using the input port (1) at F (waveguide-port) and the output port (2) at T (discrete-port).

IV. Measurement Results for The RoMLA-PATCH

To confirm the antenna characteristics for the RoMLA-PATCH, the measurement is performed using fabricated antennas. One of the fabricated RoMLA-PATCHs is shown in Fig. 14, where the patch radius is r_{PATCH} = 18.5 mm. The measured results of the gain, radiation pattern, axial ratio, and VSWR are added to Figs. 7, 10, 11, and 12, respectively, which show reasonable agreement with the simulation results.

V. IsoGE for a SqMLA Using a Coplanar Compound Method

The sections III and IV reveal the radiation characteristics for the RoMLA-RING and RoMLA-PATCH, where the LHCP gain, G_{LH}, is enhanced by a coplanar compound method, not affecting the RHCP gain (IsoGE). This section presents another discussion for the IsoGE for a square metaloop antenna, SqMLA.

A compound antenna consisting of the SqMLA and a

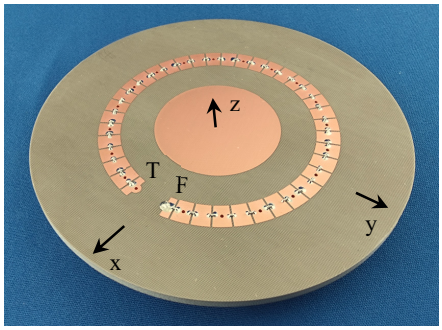

Fig. 14. An example of a fabricated RoMLA-PATCH, where the patch radius is r_{PATCH} = 18.5 mm.

conducting coplanar parasitic square patch is shown in Fig. 15, and is designated as the SqMLA-PATCH. The SqMLA is made of numerous C-type meta-atoms. Note that the meta-atom used here is already illustrated in Appendix-Fig. A, with parameters given in Appendix-Table, and is characterized by the dispersion diagram in Fig. 2. The perimeter of the SqMLA and the patch side length are denoted as C_{SqMLA} and L_{PATCH}, respectively. The center point of the patch is coincident with center point of the SqMLA. The ground plane backing the dielectric substrate is square and the side length is S_{GP} (= 110 mm).

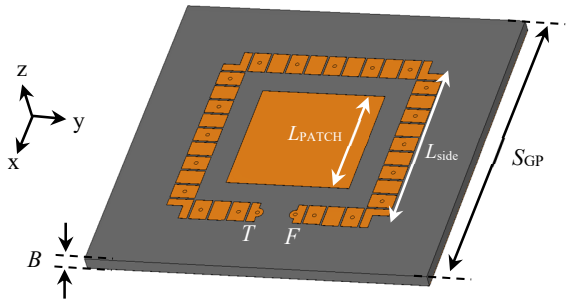

Fig. 15. Configuration of the SqMLA with a conducting coplanar patch whose side length is L_{PATCH}.

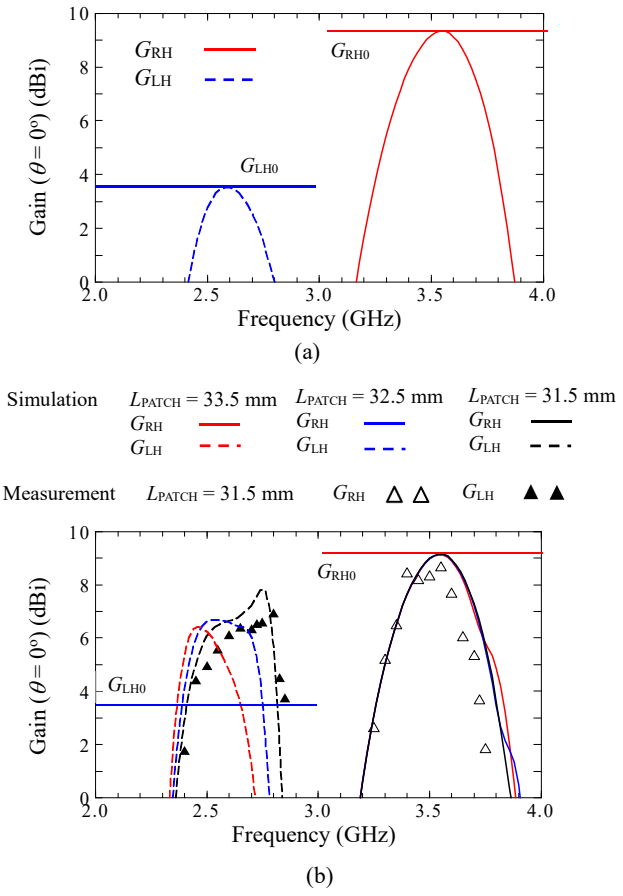

Fig. 16. Gain as a function of frequency. (a) SqMLA. (b) SqMLA-PATCH, where the patch side length (L_{PATCH}) is used as a parameter. Note that the simulated RHCP gains for three values of L_{PATCH} are almost superimposed.

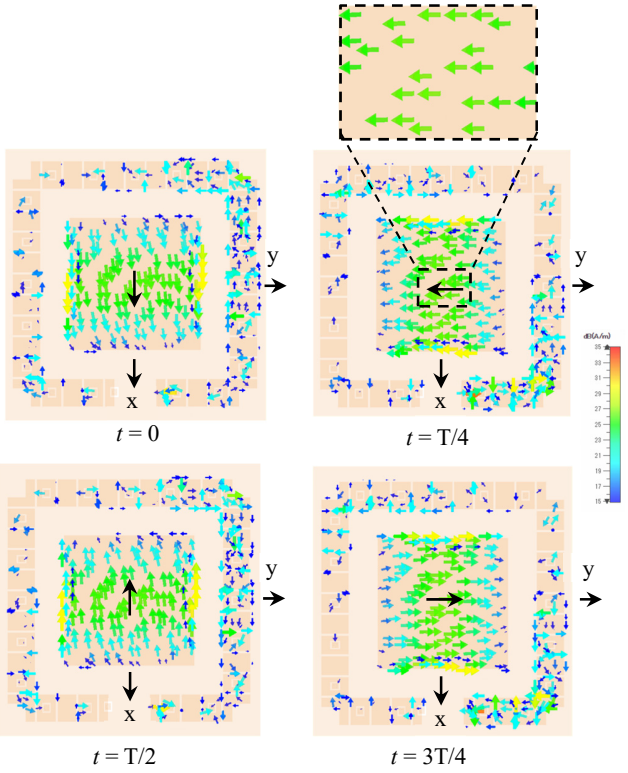

Fig. 17. Time-domain current distribution for the SqMLA-PATCH at 2.75 GHz ($\beta < 0$), where the patch side length is L_{PATCH} = 31.5 mm. T is one-time period.

Fig. 16(a) shows the frequency response of the gain for the SqMLA before the patch is inserted, where $C_{\mathrm{SqMLA}} = 4L_{\mathrm{side}}$ = 208.4 mm, which becomes $1\lambda_g$ at 2.61 GHz for $\beta < 0$ and 3.40 GHz for $\beta > 0$ in Fig. 2. It is found that gains G_{LH} and G_{RH} reach respective maximum values near these frequencies. It is also found that the maximum LHCP gain is smaller than the maximum RHCP gain: G_{LH0} = 3.5 dBi and G_{RH0} = 9.2 dBi. Fig. 16(b) shows the frequency response of the gain for the SqMLA-PATCH with patch side length L_{PATCH} as a parameter. It is revealed that G_{LH} is enhanced, while G_{RH} remains unchanged. Thus, the IsoGE for the SqMLA is realized. Note that the three values of G_{RH} are almost superimposed.

As in the case of the RoMLA-PATCH, the increase in G_{LH} is attributed to coupling of the patch to the SqMLA. For a better understanding of this fact, Fig. 17 shows one example of the TimeD J-distribution (time-domain current distribution) at 2.75 GHz, where G_{LH} for the SqMLA-PATCH is at its maximum value, with a patch side length of L_{PATCH} = 31.5 mm. It is found that the patch is coupled to the SqMLA and the current on the patch rotates clockwise due to the negative propagation phase constant ($\beta < 0$) of the current on the SqMLA. The radiation at 2.75 GHz is LHCP.

Although not illustrated, the simulation results show that there is no remarkable coupling of the patch to the SqMLA at 3.55 GHz, where the right-hand CP gain, G_{RH}, is at its maximum value. As a result, G_{RH} for the SqMLA without the patch remains unchanged, as desired. The current at this

Table IV. Square patch resonance frequency f_{eq} and simulated frequency f_{sim} for maximum G_{LH}.

L_{PATCH}	f_{eq}	f_{sim}	$\frac{f_{eq}-f_{sim}}{f_{sim}}$
33.5 mm	2.53 GHz	2.46 GHz	2.8%
32.5 mm	2.61 GHz	2.54 GHz	2.8%
31.5 mm	2.68 GHz	2.75 GHz	2.5%

frequency rotates counterclockwise due to a positive β, and the SqMLA-PATCH radiates an RHCP wave.

Finally, we estimate the frequency at which strong coupling occurs and G_{LH} reaches a maximum value. For this, we calculate the patch resonance frequency, f_{eq}, using Eq. (4) [28].

$$f_{eq} = \frac{c_0}{2\sqrt{\epsilon_r}} \left(\frac{1}{L_{PATCH}+2\Delta L_{PATCH}}\right) \quad (4)$$

where $\Delta L_{PATCH} \approx 0.5B$. Table IV shows f_{eq} for different patch side lengths, together with the maximum G_{LH} frequency, f_{sim}, obtained from Fig. 16(b) (simulation results). It is found that the difference between f_{eq} and f_{sim} is small. Hence, Eq. (4) can be used for estimating the frequency at which G_{LH} is at its maximum value, realizing the IsoGE.

VI. Conclusion

The RoMLA has the LHCP gain, G_{LH}, near nion frequency f_N, which is smaller than the RHCP gain, G_{RH}, near hion frequency f_H. To realize the IsoGE (isolated gain enhancement) for the RoMLA, a conducting parasitic ring has been inserted into the RoMLA, denoted as RoMLA-RING. When the ring is transformed into its extremity (a round patch), the patch is electromagnetically coupled to the RoMLA, and the current is generated on it, resulting in the radiation of an LHCP wave. It is found that the G_{LH} is increased, while not affecting the gain G_{RH}. Thus, the IsoGE has been realized. The parasitic patch radius and coupling frequency for such an IsoGE state are well estimated using a patch antenna operating in the TM^z_{110} mode. The measurement results, including the gain, radiation pattern, axial ratio, and VSWR of the C-RoMLA with the patch show reasonable agreement with the simulation results.

Further investigation has revealed that an SqMLA with a parasitic patch (SqMLA-PATCH) has an increased LHCP gain with almost unchanged RHCP gain. Thus, the IsoGE for the SqMLA has been realized. It is found that the parasitic square patch size for the IsoGE can be estimated by the size of a fed square patch antenna.

Appendix

C-type meta-atom

A section of length p_{atm} shown in Appendix-Fig. A is called a C-type meta-atom, which is supported by a grounded dielectric substrate of thickness B and relative permittivity ε_r. Notation p_0 is the length of a conducting small strip and notation g is the gap between neighboring strips. A chip element of

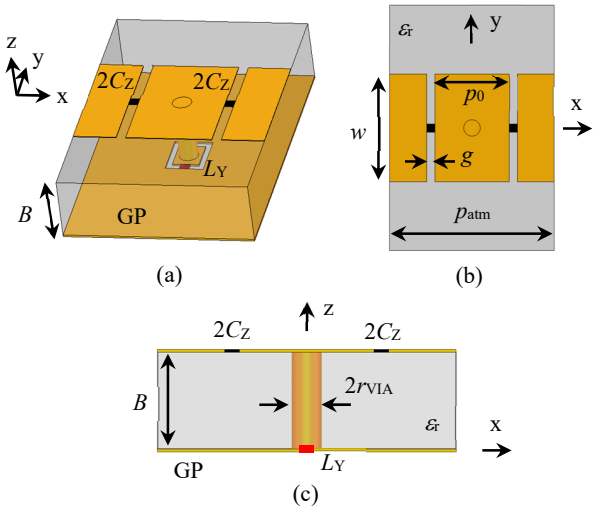

Appendix-Fig. A. C-type meta-atom. (a) Perspective view. (b) Top view. (c) Side view.

Appendix-Table. Parameters for C-type meta-atom.

Symbol	Value	Symbol	Value
B	3.2 mm	ε_r	2.6
p_{atm}	10 mm	w	6.6 mm
p_0	4.5 mm	g	0.5 mm
$2r_{VIA}$	1.0 mm	L_Y	1.8 nH
$2C_Z$	1.2 pF		

inductance L_Y is inserted between the ground plane, GP, and the end of a conducting pin of diameter $2r_{VIA}$, which extends vertically from the center strip of length p_0; a chip element of capacitance $2C_Z$ is inserted into the gap of g.

Appendix-Table presents the parameters for the C-type meta-atom used in this paper, which are optimized such that the transition frequency, f_T, is 3 GHz, as shown by the dispersion diagram in Fig. 2, where β is the propagation phase constant of the current on the C-type meta-atom and k_0 is the wave number in free space.

Acknowledgment

The authors thank V. Shkawrytko for his assistance in the preparation of this manuscript. This work was supported in part by the Japan Society for the Promotion of Science (JSPS) KAKENHI under Grant JP21K04068.

References

[1] J. Kraus, R. Marhefka, *Antennas*, 3rd edition, McGraw Hill, NY, 2002.
[2] C. A. Balanis, *Antenna Theory: Analysis and Design*, 2nd edition, Wiley, NY, 1982.
[3] Z. N. Chen, D. Liu, H. Nakano, X. Qing, and T. Zwick (Eds), *Handbook of antenna Technologies*, Springer Singapore, 2016.
[4] K. Hirasawa, *Antenna Characteristics and Fundamental Antenna Analysis Tecnologies*, Nikkankogyoshinbun, 2011 (Japanese).
[5] H. Nakano, K. Nogami, S. Arai, H. Mimaki, and J. Yamauchi, "A spiral antenna backed by a conducting plane reflector," IEEE Trans. Antennas Propagat., vol. 34, no. 6, pp. 791-796, June, 1986.
[6] D. Sievenpiper, L. Zhang, R. Broas, N. Alexopolous, and E. Yablonovitch, "High-impedance electromagnetic surfaces with a forbidden frequency band," IEEE Trans. MTT, vol. 47, no. 11, pp. 2059-2074, 1999.

[7] P. Deo, A. Mehta, D. Mirshekar-Syahkal, P. J. Massey, and H. Nakano, "Thickness reduction and performance enhancement of steerable square loop antenna using hybrid high impedance surface," IEEE Trans. Antennas Propagat., vol. 58, no. 5, pp. 1477-1485, May, 2010.
[8] D. Nashaat, H. Elsadek, E. A. Abdallah, M. F. Iskander, and H. M. Elhenawy, "Ultrawide bandwidth 2x2 microstrip patch array antenna using electromagnetic band-gap structure (EBG)," IEEE Trans. Antennas Propagat., vol. 59, no. 5, pp. 1528-1534, May 2011.
[9] F. Yang and Y. Rahmat-Samii, "A low-profile circularly polarized curl antenna over an electromagnetic bandgap (EBG) surface," Microw. Opt. Tech. Lett., vol. 31, pp. 264–267, Nov. 2001.
[10] H. Nakano, Y. Asano, and J. Yamauchi, "A wire inverted F antenna on a finite-sized EBG material," IEEE Int. Workshop on Antenna Technology, iWAT, pp. 13-16, Singapore, March 2005.
[11] C. Caloz and T. Itoh, *Electromagnetic Metamaterials,* Wiley, NJ, 2006.
[12] G. Eleftheriades and K. Balmain, *Negative-Refraction Metamaterials: Fundamental Principles and Applications*. New York: Wiley-IEEE Press, 2005.
[13] N. Engheta and R. W. Ziolkowski, *Electromagnetic Metamaterials*: *Physics and Engineering Explorations*. New York: Wiley-IEEE Press, 2006.
[14] H. Nakano, *Low-profile Natural and Metamaterial Antennas*, Wiley-IEEE Press, NJ, 2016.
[15] H. Nakano, K. Sakata, and J. Yamauchi,"Linearly and circularly polarized radiation from metaline antennas," iWAT, pp. 142-143, Cocoa Beach, FL, USA, Feb. 2016.
[16] H. Nakano, K. Yoshida, and J. Yamauchi, "Radiation characteristics of a metaloop antenna," IEEE AWPL, vol. 12, pp. 861-863, 2013.
[17] H. Nakano, I. Yoshino, T. Abe, and J. Yamauchi, "Balanced gain for a square metaloop antenna," EPJ Appl. Metamat., vol. 6, no. 3, pp. 1-5, 2019.
[18] H. Nakano, T. Abe, and J. Yamauchi, "Compound metaloop antenna for circularly polarized beam steering," IEEE Access, vol. 9, pp. 79806-79815, June 2021.
[19] H. Nakano, T. Abe, and J. Yamauchi, "Circularly polarized broadside beam radiated from a large, low-profile metaloop antenna," IEEE Trans. Antennas Propagat., vol 71, no. 1, pp. 29-38, Jan. 2023.
[20] H. Nakano, T. Abe, and J. Yamauchi, "Theoretical investigation of radiation in the normal direction for a metaloop antenna," IEEE Access, vol. 8, pp. 122826-122837, July 2020.
[21] H. Nakano, T. Abe, A. Mehta, and J. Yamauchi, "Compound metacurl antenna with C- and N-type metaatoms," IEEE Access, vol. 8, pp. 51703-51712, March 2020.
[22] CST Computer Simulation Technology GmbH, Darmstadt, Germany, Microwave Studio. [Online]. Available: http://www.cst.com, Accessed on: Aug. 2022.
[23] K. Ding, C. Gao, T. Yu, D. Qu, and B. Zhang, "Gain-improved broadband circularly polarized antenna array with parasitic patches," IEEE AWPL, vol. 16, pp. 1468-1471, 2017.
[24] K. Ding, C. Gao, D. Qu, and Q. Yin, "Compact broadband circularly polarized antenna with parasitic patches," IEEE Trans. Antennas Propagat., vol. 65, no. 9, pp. 4854-4857, Sept. 2017.
[25] J. Wu, Y. Yin, Z. Wang and R. Lian, "Broadband circularly polarized patch antenna with parasitic strips," IEEE AWPL, vol. 14, pp. 559-562, 2015.
[26] W. Yang and J. Zhou, "Wideband circularly polarized cavity-backed aperture antenna with a parasitic square patch," IEEE AWPL, vol. 13, pp. 197-200, 2014.
[27] L. Leszkowska, M. Rzymowski, K. Nyka, and L. Kulas, "High-gain compact circularly polarized X-band superstrate antenna for CubeSat applications," IEEE AWPL, vol. 20, no. 11, pp. 2090-2094, Nov. 2021.
[28] D. Jackson, *Introduction to a microstrip antennas*, Short course at IEEE APS, Orlando, Florida, July 2013.

Hisamatsu NAKANO (M'75–SM'87–F'92–LF'11) has been with Hosei University since 1973, where he is currently a Professor Emeritus and a Special-appointment Researcher with the Electromagnetic Wave Engineering Research Institute attached to the graduate school. He has held positions as Visiting Associate Professor at Syracuse University (March to September 1981), Visiting Professor at the University of Manitoba (March to September 1986), University of California, Los Angeles (September 1986 to March 1987), and Swansea University, U.K. (July to September of 2016 to 2019 and 2022). He has published over 370 articles in peer-reviewed journals and 11 books/book chapters, including *Low-profile Natural and Metamaterial Antennas* (IEEE Press, Wiley, 2016). His significant contributions are the development of five integral equations for line antennas in free space and printed on a dielectric substrate, the invention of an L-shaped wire/strip antenna feeding method, and the realization of numerous wideband antennas, including curl, metaspiral, metahelical, and Body of Revolution antennas. His other accomplishments include design of antennas for GPS, personal handy phones, space radio, electronic toll collection, RFID, UWB, and radar. He has been awarded 79 patents, including *A Curl Antenna Element and Its Array* (Japan). He served as a member of the IEEE APS Administrative Committee from 2000 to 2002 and a Region 10 Representative from 2001 to 2010. He received the H. A. Wheeler Award in 1994, the Chen-To Tai Distinguished Educator Award in 2006, and the Distinguished Achievement Award in 2016, all from the IEEE Antennas and Propagation Society. He was also a recipient of The Prize for Science and Technology from Japan's Minister of Education, Culture, Sports, Science and Technology in 2010. Most recently, he was selected as a recipient of the Antenna Award of the European Association on Antennas and Propagation (EurAAP) in 2020. He is an Associate Editor of several scientific journals and magazines, including Electromagnetics.

TOMOKI ABE (M'19) was born in Miyagi, Japan, on August 12, 1994. He received the B.E., M.E., and Ph.D. degrees in Electronics and Electrical Engineering from Hosei University, Tokyo, Japan, in 2017, 2019, and 2022, respectively. Mr. Abe is a member of the Institute of Electronics, Information and Communication Engineers of Japan.

AMIT MEHTA (M'05 - SM'11) received the B.Eng. degree in electronics and telecommunication from the University of Pune, India, in 1998 and the M.Sc. degree in telecommunications and information networks and the Ph.D. degree in smart reconfigurable antennas from the University of Essex, U.K., in 2002 and 2005, respectively. From 1998 to 2001, he worked in the Telecommunications Industry in Bangalore and Singapore. From July 2002 to February 2006, he was a Senior Research Officer at the University of Essex. Since February 2006, he has been working at Swansea University, Swansea, U.K. and is the director of the RF research group where his core research focus is wireless communications, microwave systems and antennas. He is particularly interested in GNSS, body-wearable adaptable antennas, satellite communications, smart antennas, 4G, and millimeter waves. He has successfully supervised over 20 postgraduate research theses and has over 80 technical publications and three patents on invention of the steerable beam smart antenna and concealed weapons detection system.

JUNJI YAMAUCHI (M'84–SM'08–F'12-LF'19) was born in Nagoya, Japan, on August 23, 1953. He received the B.E., M.E., and Dr. E. degrees from Hosei University, Tokyo, Japan, in 1976, 1978, and 1982, respectively. From 1984 to 1988, he served as a Lecturer in the Electrical Engineering Department, Tokyo Metropolitan Technical College. Since 1988, he has been a member of the faculty of Hosei University, where he is now a Professor at the Electrical and Electronic Engineering Department. His research interests include optical waveguides, polarization converters, and circularly polarized antennas. He is the author of "*Propagating Beam Analysis of Optical Waveguides* (Research Studies Press, 2003)." Dr. Yamauchi is a member of the Optical Society of America and the Institute of Electronics, Information and Communication Engineers of Japan.